ICSV13 - Vienna
The Thirteenth International Congress on Sound and Vibration
Vienna, Austria, July 2-6, 2006

THE PLATE IMPINGEMENT OF THE WEAK SHOCK WAVE DISCHARGING FROM VARIOUS 3-DIMENSIONAL DUCTS

Y.-H. Kweon*[1], C.-M. Lim[4], Y. Miyazato[3], T. Aoki[2], H.-D. Kim[4], T. Setoguchi[5] and S. Matsuo[5]

[1]JSPS Research Fellow PD (Dept. Energy and Environmental Engg., Kyushu Univ.)
[2]Department of Energy and Environmental Engineering, Kyushu University
6-1 Kasuga kouen, Kasuga, Fukuoka 816-8580, Japan
[3]Faculty of Environmental Engineering, The University of Kitakyushu
1-1 Hibikino, Wakamatsu-ku, Kitakyushu 808-0135, Japan
[4]School of Mechanical Engineering, Andong National University
388 Songchun-dong, Andong, Kyungpuk 760-749, Korea
kimhd@andong.ac.kr
[5]Department of Mechanical System Engineering, Saga University
1 Honjo-machi, Saga 840-8502, Japan

Abstract

This paper describes computational work to understand the unsteady flow-field of a shock wave discharging from an exit of a duct and impinging upon a plate plane. A flat plate is located downstream, and normal to the axis of the duct. The distance between the exit of the duct and flat plate is changed. In the present study, two different duct geometries (i.e., square and cross section) are simulated to investigate the duct geometry effect on the unsteady flows of a shock wave. In computation, the TVD scheme is employed to solve three-dimensional, unsteady, compressible Euler equations. Computations are performed over the range of shock Mach number from 1.05 to 1.75. The results obtained show that the pressure increase generated on the plate by the shock impingement depends on the duct geometry and the distance between the duct exit and plate, as well as the shock Mach number. It is also found that for the duct with cross-section, the unsteady loads acting on the plate are less, compared with the square duct.

INTRODUCTION

When a gas is suddenly discharged from an exit of a duct or pipe, the pulse jet is formed at the vicinity of the exit of a duct. If the mass flux discharged is sufficiently large, the pulse jet leads to a strong impulse wave which propagates toward surroundings. Simi-

lar flows are made by the discharge of a shock wave from the exit of a duct, leading to an impulse wave that is usually characterized by a high peak pressure of short duration. Compared with the noise of a subsonic or a supersonic steady jet discharged from a nozzle, the noise due to such an impulse wave often causes large, undesirable, unsteady loads and pressure transients which are a major source of structural vibration and fatigue of a mechanical system. In some industrial manufacturing processes, it results in a serious hearing problem to workers [1]. It is required that the impulse wave should be minimized by an appropriate control means.

There have been a number of practical applications in which a stronger impulse wave casts a better performance of the fluidic devices, such as pulse combustors [2], pulse jet filters [3], pulse jet cleanings [4], etc. The pulse jet devices for such purposes are now in commercial production or have recently been used for a variety of industrial fields. For example, in the semiconductor industry or coal-based power plants, removal of fine particles from surfaces is of practical importance both for surface cleaning and for contamination detection [5].

Until now, for the flow fields produced by the steady jet impinging upon an object, a lot of researches have been carried out. In 1985, Krothapalli [6] studied the discrete tones generated by a supersonic jet impinging upon a flat plate, and reported the variations in both flow- and acoustic fields. Henderson [7] studied the connection between sound production and structure of a jet impinging upon a flat plate.

Meanwhile, the current understanding of the unsteady flow fields due to the shock wave impinging upon an object is not enough for the purpose of design of practical applications. In such applications, it is of practical importance to predict the pressure transients and unsteady loads on an object. To the author's knowledge, only a few efforts to date have been put on this field. For example, Setoguchi et al. [8] studied the impingement of impulse wave upon a flat plate. They showed that when the shock wave discharged from a tube is impinging upon a flat plate, a sharp peak of very short rising time is generated at the plate plane, and its magnitude depends upon the distance between the exit of a tube and plate.

The present paper describes computational work to understand the unsteady flow -fields formed by the plate impingement of shock wave discharging from various three-dimensional ducts. Computations are performed to solve the three-dimensional, unsteady, compressible, Euler equations. The total variation diminishing (TVD) scheme is used to discretize the governing equations. The effects of the duct geometry and the distance between the exit of a duct and flat plate on the unsteady flow-fields of the shock wave are investigated in detail.

COMPUTATIONAL ANALYSIS

Governing Equations

In order to simulate the shock wave discharging from the duct exit and impinging on the plate, the unsteady, three-dimensional, compressible, Euler equations are employed in the present computation. The governing conservation equations are given by

$$\frac{\partial U}{\partial t}+\frac{\partial E}{\partial x}+\frac{\partial F}{\partial y}+\frac{\partial G}{\partial z}=0,$$

$$U=\begin{bmatrix} r \\ ru \\ rv \\ rw \\ e \end{bmatrix},\quad E=\begin{bmatrix} ru \\ ru^2+p \\ ruv \\ ruw \\ (e+p)u \end{bmatrix},\quad F=\begin{bmatrix} rv \\ ruv \\ rv^2+p \\ rvw \\ (e+p)v \end{bmatrix},\quad W=\begin{bmatrix} rw \\ ruw \\ rvw \\ rw^2+p \\ (e+p)w \end{bmatrix} \tag{1}$$

where t is time, ρ is the density and u, v and w are the velocity components in the x, y and z directions, respectively. The total energy e per unit volume of the gas is expressed as $e=p/(\gamma-1)+\rho(u^2+v^2+w^2)/2$.

Equation (1) is closed by the thermal equation of the state of a perfect gas, $p=\rho RT$, where T is the temperature. In computation, Eq.(1) is rewritten in non-dimensional form by referring the quantities to atmospheric conditions as follows :

$$p'=\frac{p}{p_1},\quad r'=\frac{r}{r_1},\quad u'=\frac{u}{a_1\sqrt{g}},\quad v'=\frac{v}{a_1\sqrt{g}},\quad w'=\frac{w}{a_1\sqrt{g}},\quad t'=\frac{t}{(D/a_1)\sqrt{g}},$$

$$x'=\frac{x}{D},\quad y'=\frac{y}{D},\quad z'=\frac{z}{D} \tag{2}$$

where the subscript 1 indicates the atmospheric condition, D the equivalent diameter of a duct and a the speed of sound. If the symbol ($'$) indicating the non-dimensional quantities is omitted for the sake of simplicity, then the equation system is exactly equivalent to Eq.(1). For the present computational analysis, the Yee-Roe-Davis's TVD scheme [9] is applied to solve the governing equations. An operator splitting technique, suggested by Sod [10], is employed in the present computation.

Computational Domain and Boundary Conditions

In the present computation, two different duct geometries (see Fig.1) are applied to investigate the effect of duct geometry on the flow-fields formed by the shock wave. In Fig.1(b), the duct exit with cross-section has closed by approximately 50%, compared with the exit area of square duct.

Figure 2 shows the computational domain and boundary conditions employed in computation. As an initial condition for computation, an incident, normal shock wave of Mach number M_s is assumed at x/D=-0.5 inside the duct where x/D=0 indicates the duct exit plane. The incident shock wave propagates toward the open end of a duct and is eventually discharged from the exit of a duct toward surroundings. As shown in Fig.2, the computational domain is composed of the duct and flat plate located downstream. As the inflow and outflow boundary conditions, the zeroth-order extrapolation is used for the conservative variables. The boundary conditions on all the surfaces inside and outside of the duct and the plate surface are the slip-wall conditions. A structured grid system with square cells is used in computation. The grid density effect on the com-

puted solutions is first investigated and the computational grids over 1,100,000 seem to be fairly good for the present computations.

The Mach number (M_s) of the incident shock wave is changed between 1.05 and 1.75. The distance (L) between the exit of a duct and plate plane is varied from 0.5D to 2.5D. In order to understand the effects of M_s and L on the flow-field, the pressure fluctuations on the plate plane due to the shock impingement and the computed flow visualization are obtained from the computations.

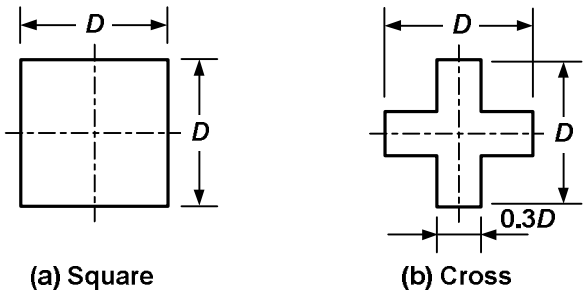

Figure 1 – Duct exit geometries applied in computation

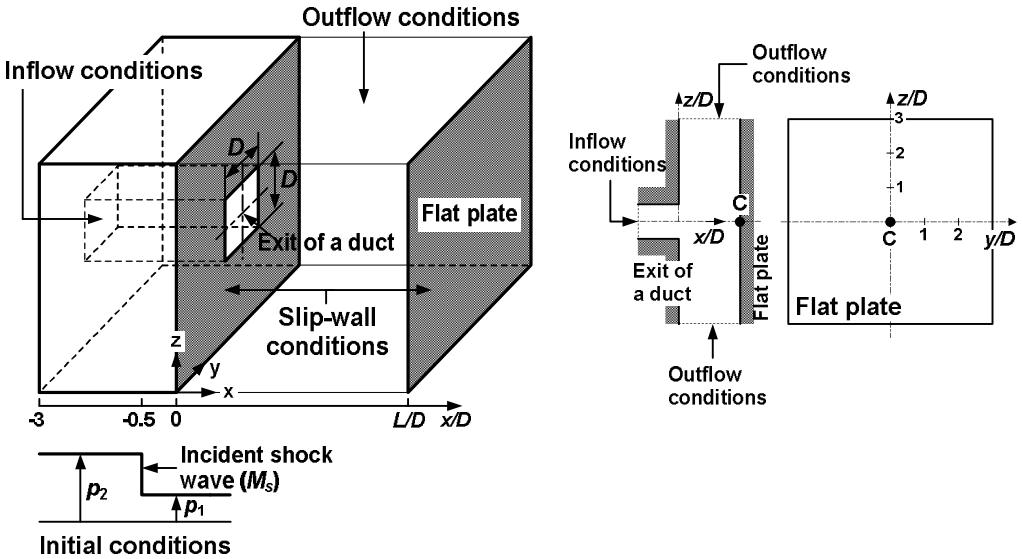

Figure 2 – Computational domain and boundary conditions

RESULTS AND DISCUSSION

Figures 3 and 4 show the computed iso-pressure contours showing the shock waves discharging from the exits of two different ducts and impinging upon the flat plate for M_s=1.25 and L/D=1.0. The non-dimensional time t' is taken to be zero for the incident shock wave at x/D=-0.5. At t'=0.79, the shock wave (S) discharged from the exit of a square duct is just impinging upon the flat plate, as shown in Fig.3(a). At the corner of the duct exit, the shock wave diffraction and vortical structure (V) are observed. It is also observed that the expansion waves (E) propagates back inside the duct. At t'=1.67,

the wave form is taken for an instance after the shock wave impinged upon the flat plate. The reflected shock wave (RS) from the plate propagates upstream toward the duct. The interaction (SS) between a part of the reflected shock and vortical structures is clearly observed. With an increase in time, the vortical structure grows gradually, propagating toward downstream. For yz-plane at *x/D*=0, the unsteady flow-fields are shown in Fig.3(b). At *t'*=0.79, the outer and inner black loops indicate the shock wave (S) and vortical structure (V), respectively. As shown in Fig.3(b), the initial wave form discharged from the exit of a duct is nearly square. However, when the time elapses, the wave form is changed to spherical, propagating toward surroundings.

In Fig.4, the dynamic behaviours of shock wave discharged from the exit of a cross-type duct are similar to those of the square duct. However, it seems that both the shock wave (S) and the reflected shock (RS) are weaker than those of the square duct, while the vortical structure is stronger.

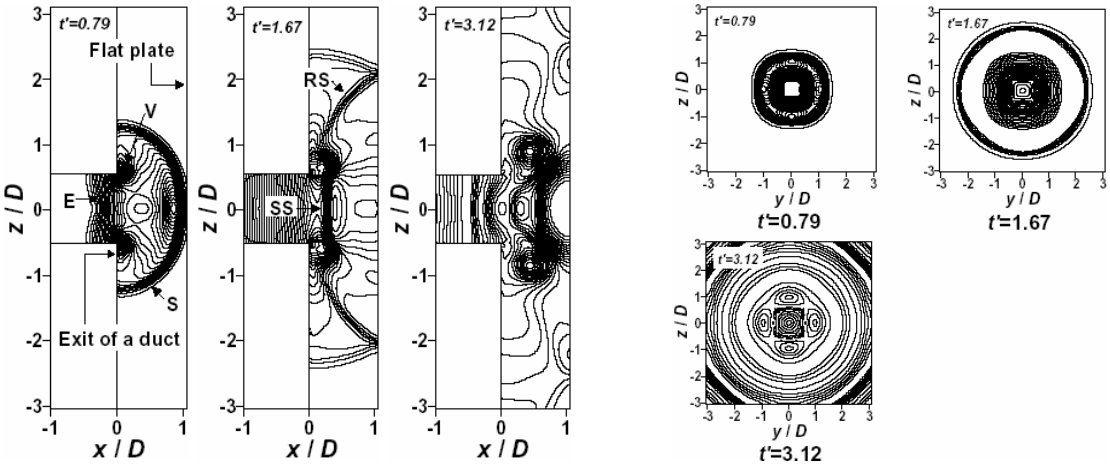

(a) *xz*-plane (*y/D*=0) (b) *yz*-plane (duct exit plane - *x/D*=0)

Figure 3 – Computed iso-pressure contours for the square exit (M_s=1.25, L/D=1.0)

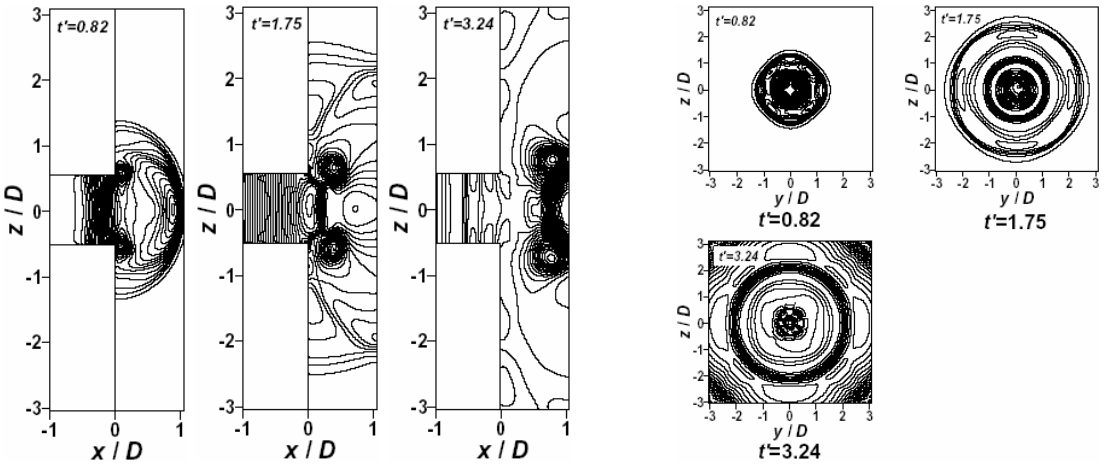

(a) *xz*-plane (*y/D*=0) (b) *yz*-plane (duct exit plane - *x/D*=0)

Figure 4 – Computed iso-pressure contours for the cross exit (M_s=1.25, L/D=1.0)

Figure 5 shows the detailed pressure distribution generated on the plate plane by the shock impingement. Although the time t' a little differs in each case, the pressure values for the cross duct are lower than those of the square duct. It is also found that the low pressure and sunken region indicating the vortical structure appears more widely, compared with that of the square duct.

Figure 6 shows the pressure-time histories at the central point (symbol C in Fig.2) of the plate. In Fig.6(a), the pressure on the flat plate suddenly rises up to a peak value, strongly depending on the duct geometry. After the peak value, the pressure sharply decreases with time, and then increases again due to the shock-shock interactions in the region between the duct exit and plate plane. The relationship between the first peak value and shock Mach number is shown in Fig.6(b). The first peak value increases with the shock Mach number. For the cross duct, the first peak pressure is lower than that of the square duct. It is believed that the duct with cross-section can effectively lead to the reduction of unsteady loads acting on the plate plane due to the shock impingement.

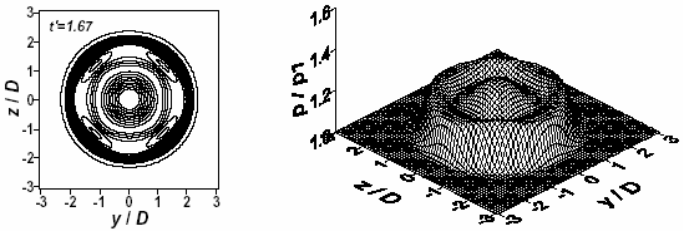

(a) Square (*yz*-plane, *x/D*=1.0)

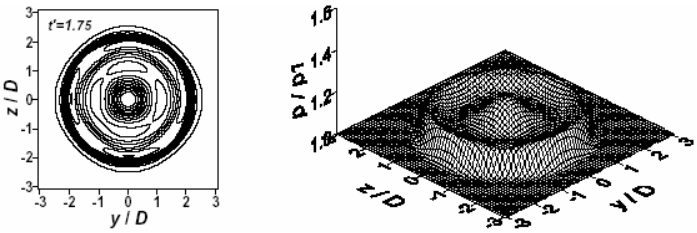

(b) Cross (*yz*-plane, *x/D*=1.0)

Figure 5 – Computed iso-pressure contours on the flat plate (M_s=1.25, L/D=1.0)

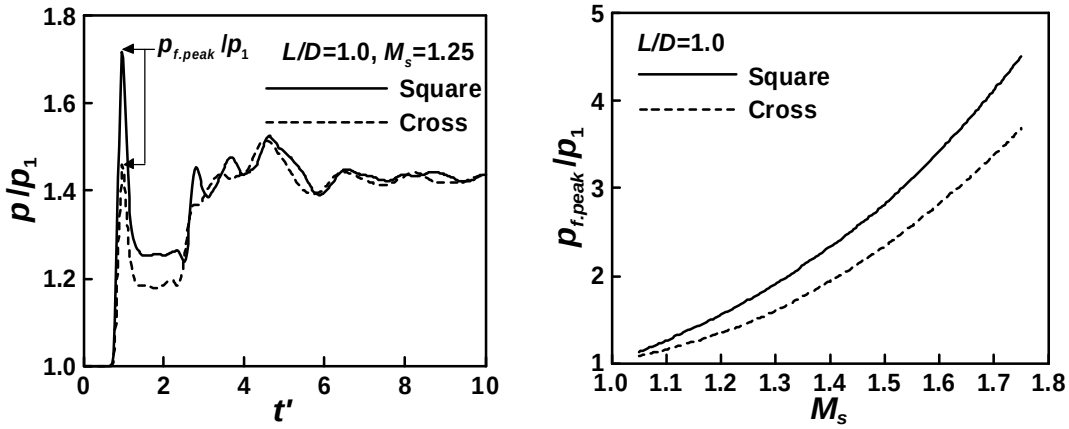

(a) Pressure-time history (b) The first peak value vs M_s

Figure 6 – Effect of M_s on the first peak pressure at the central point of flat plate (C)

The effect of the distance (*L/D*) between the duct exit and plate on the first peak pressure of the plate is shown in Fig.7. In Fig.7(a), the *L/D* value considerably affects both the first peak value and the pressure rise after the first peak value. For example, this pressure rise for *L/D*=1.5 is remarkably higher than the first peak value. The first peak pressure decreases with an increase in *L/D*, as shown in Fig.7(b).

Figure 8 shows the peak pressure distribution along the z-axis on the plate. As shown in Fig.7(a), the pressure value at a certain place of the plate plane is transient with time. In order to obtain the peak pressure distribution on the plate, the local peak pressures are taken for each time step during computations. The peak pressure distribution along the z-axis on the plate plane is shown in Fig.8(a). The maximum value of the peak pressure appears at the central point of the plate (*y/D*=0, *z/D*=0). The peak pressure decreases with the distance in radial direction. The peak pressures for the duct with cross-section are lower than those of the square duct over the entire plate plane. The comparison between the first peak and maximum pressure at the central point of

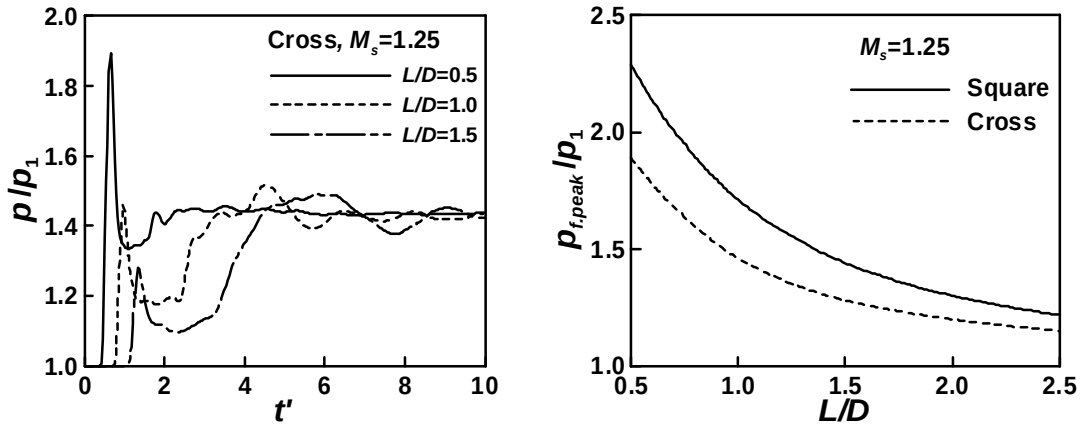

(a) Pressure-time history (b) The first peak value vs *L/D*

Figure 7 – Effect of L/D on the first peak pressure at the central point of flat plate (C)

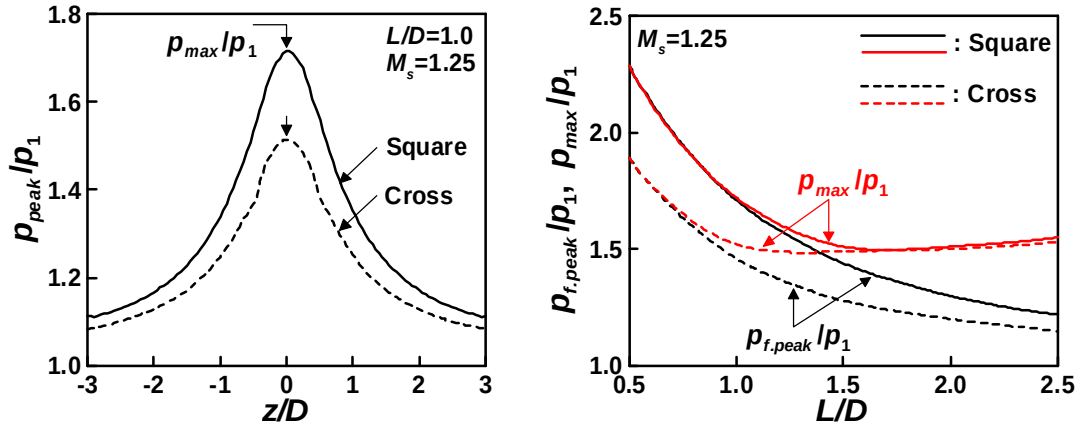

(a) Peak pressure distribution along *z/D on flat plate (x/D=1.0, y/D=0)* (b) Maximum pressure vs *L/D*

Figure 8 – Comparison between the first peak and maximum pressures at the central point of flat plate (C)

the flat plate is shown in Fig.8(b). As readier shown in Fig.7(b), the first peak pressure gradually decreases with *L/D*. For *L/D*<1.0, the maximum pressure is nearly the same with the first peak pressure. However, for *L/D*>1.0, the maximum pressure has nearly a constant value that is higher than the first peak value, regardless of *L/D* value.

CONCLUSIONS

This paper describes computational work to understand the unsteady flow-fields of a shock wave discharging from an exit of a duct and impinging upon a plate plane. A flat plate is located downstream, and normal to the axis of the duct. The distance between the exit of the duct and flat plate is changed. In the present study, two different duct geometries (i.e., square and cross section) are simulated to investigate the effect of the duct geometry on the unsteady flows of shock wave. In computation, the TVD scheme is employed to solve three-dimensional, unsteady, compressible, Euler equations. Com -putations are performed over the range of shock Mach number from 1.05 and 1.75. Computational results can predict the three-dimensional dynamic behavior of the shock wave impinging upon the flat plate. The results obtained show that the pressure increase generated on the plate plane by the shock impingement depends on the duct geometry and the distance between the duct exit and plate, as well as the shock Mach number. It is also found that for the duct with cross-section, the unsteady loads acting on the plate plane are less, compared with those of the square duct.

REFERENCES

[1] Rice, C.G., “Human Response Effects of Impulse Noise”, J. Sound and Vibration, **190** (3), 525-543 (1996).

[2] Kentfield, J.A.C., *Nonsteady, One-Dimensional, Internal, Compressible Flows (Theory and Applications.* (Oxford : Oxford University Press, Chapter 7, 1993).

[3] Klingel, R., Loffler, F., “Dust Collection and Cleaning Efficiency of a Pulse Jet Fabric Filters”, Proceedings of the Filtration Society, Filtration and Separation, **20**, 205-208 (1983).

[4] Morris, W.J., “Cleaning Mechanism in Pulse Jet Fabric Filters”, Proceedings of the Filtration Society, Filtration and Separation, **21**, 52-54 (1984).

[5] Smedly, G.T., Phares, D.T., Flagan, R.C., “Entrainment of Fine Particles from Surfaces by Impinging Shock Waves”, Experiments in Fluids, **26**, 116-125 (1998).

[6] Krothapalli, A., “Discrete Tones Generated by an Impinging Underexpanded Rectangular Jet”, AIAA J., **23** (2), 1910-1915 (1985).

[7] Henderson, B., “The Connection between Sound Production and Jet Structure of the Super -Sonic Impinging Jet”, J. Acoust. Soc. Am., **111** (2), 735-747 (2002).

[8] Setoguchi, T., Kim, H.-D., Kashimura, H., “Study of the Impingement of Impulse Wave upon a Flat Plate”, J. Sound and Vibration, **256** (2), 197-211 (2002).

[9] Yee, H.C., “Upwind and Symmetric Shock Capturing Schemes”, NASA TM-89464 (1987).

[10] Sod, G.A., “A Numerical Study of a Converging Cylindrical Shock”, J. Fluid Mechanics, **83**, 785-794 (1977).